THE JOURNAL OF PHYSICAL CHEMISTRY A
A JOURNAL OF THE AMERICAN CHEMICAL SOCIETY

pubs.acs.org/JPCA Article

Dissociative Photoionization of Chloro-, Bromo-, and Iodocyclohexane: Thermochemistry and the Weak C−Br Bond in the Cation

Xiangkun Wu, Xiaoguo Zhou,* Patrick Hemberger, and Andras Bodi*

Cite This: J. Phys. Chem. A 2021, 125, 646−656 Read Online

ACCESS | Metrics & More | Article Recommendations

ABSTRACT: Double-imaging photoelectron photoion coincidence spectroscopy (i^2PEPICO) with tunable synchrotron vacuum ultraviolet radiation was used to record threshold ionization mass spectra of the halocyclohexanes $C_6H_{11}X$ (X = Cl, Br, and I). Calculations show that experimental dissociative ionization thresholds correspond to thermochemical limits. Among the processes observed (X loss, followed by C_2H_4 or C_3H_6 loss; C_2H_3Cl loss; HCl loss, followed by CH_3 or C_2H_4 loss), halogen atom loss can be used to derive enthalpies of formation and C−X bond energies in the cation. As an ancillary value, we propose a new proton affinity for cyclohexene at $PA_{298K}(c\text{-}C_6H_{10})$ = 771.5 ± 1.7 kJ mol^{-1}. The halogen loss onsets 10.74 ± 0.06 eV, 10.125 ± 0.005, and 9.474 ± 0.005 eV thus yield $\Delta_f H°_{298K}(C_6H_{11}X\ (g))$ = −164.4 ± 6.2, −114.4 ± 2.3, and −56.3 ± 2.3 kJ mol^{-1} for X = Cl, Br, and I, respectively. The last two agree with DFT-calculated isodesmic reaction energies very well, as opposed to G4 theory for X = Br. The C−X bond energy in the cation is the lowest for X = Br. This is the sum result of the weakening C−X bond in the neutral and the increasing stabilization of the parent ion with increasing halogen size.

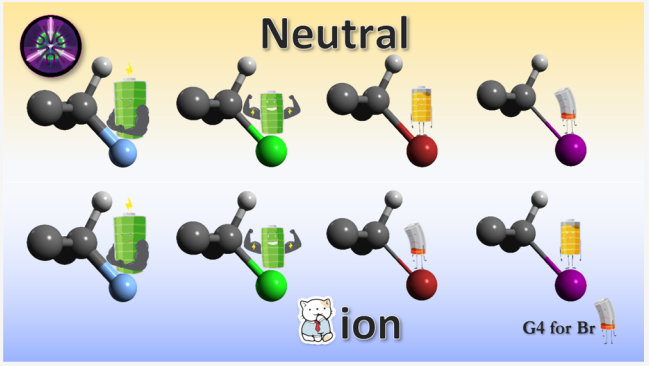

1. INTRODUCTION

Reaction mechanisms are governed by short-lived reactive intermediates connected by ephemeral transition states. Velocity map (double) imaging photoelectron photoion coincidence spectroscopy[1] (i^2PEPICO) represents a universal, multiplexed, sensitive, and selective approach to detect and identify elusive intermediates in complex reaction mixtures.[2] The photoion mass-selected photoelectron spectrum often exhibits a vibrational fine structure and allows for isomer-specific assignment, which then helps establish the reaction mechanism, for example, in bimolecular processes relevant in combustion and astrochemistry[3] or in catalysis.[4,5]

Conformer-specific reactivity was observed, for example, in the photolysis of the 1-iodopropane[6] and propanal[7] ions and in thiophenols[8] and the dissociative photoionization (DPI) of alanine.[9] This was the reason why we set out to apply PEPICO to monosubstituted cyclohexanes, one of the prototypical examples for conformational isomerism.[10] They have two distinct low-energy conformers, the equatorial (*eq*-) and axial (*ax*-) chair structures, with lifetimes on the order of microseconds at room temperature and years at −150 °C.[11] The equatorial preference for larger ligands is typically attributed to steric effects, but hyperconjugation plays just as an important role.[12] Furthermore, dispersion interaction governs the systematic,[13] albeit counterintuitive, changes in the silacyclohexane conformation behavior.[14] The analysis of the threshold photoelectron spectrum (TPES) and the breakdown diagram of halosilacylohexanes revealed little about their conformers but shed light on the electronic structure and the effect of silicon on the bonding of the molecule. The strong silicon−halogen bond, together with silicon's greater propensity to small bond angles, opens up unusual fragmentation pathways and results in the electrophilic halogen staying trapped in the cation.[15] The TPES of fluorocyclohexane, on the other hand, was clearly found to be conformer-dependent.[16] It also revealed that the excitation energy to the first electronic excited state is 0.03 eV *vs* 0.3 eV in the otherwise almost isoenergetic axial and equatorial cation, respectively. Thus, large electronic structure changes may accompany conformational isomerism even when the energy change is negligible. We also located the conical intersections

Received: November 18, 2020
Revised: December 23, 2020
Published: January 11, 2021

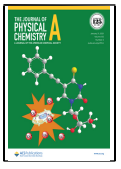

https://dx.doi.org/10.1021/acs.jpca.0c10386
J. Phys. Chem. A 2021, 125, 646−656

coupling the low-lying electronic states and identified the conformer-specific spectral fingerprints of the heavier monohalogenated cyclohexanes by equation-of-motion-coupled cluster ionization energy calculations and Franck−Condon simulations of the TPES.[17] Thus, PEPICO was confirmed to be a conformer-selective detection tool.

Using monochromatic vacuum ultraviolet ionizing radiation and discriminating for threshold, that is, near-zero kinetic energy electrons, we control the photoionization energy balance and can tune the internal energy deposited in the parent ion and available for fragmentation.[1,18] This allows us to reveal the dissociative photoionization (DPI) mechanism and accurate activation energies by statistical modeling,[19] as shown for 1-iodoalkanes, halosilacyclohexanes, fluorocyclohexane, or bromobutyne isomers.[14,16,20,21] Furthermore, if the dissociative photoionization onsets correspond to the thermochemical threshold, they can also be used in an ion cycle to derive accurate enthalpies of formation, as was carried out for the C_3H_5Br isomers.[22] We expected the halogen loss fragment to show up in chlorocyclohexane and were sure that it would drive the DPI mechanism in bromo- and iodocyclohexane based on calculations, the analysis of electron ionization mass spectra, and previous photoionization mass spectrometry experiments by Sergeev *et al.*[15,23] Therefore, we decided to go beyond the original motivation of the cyclohexane studies of conformer-selective detection and the conformer dependence of the electronic structure. Here, we plot and model the breakdown diagram of chloro-, bromo-, and iodocyclohexane, determine accurate halogen-loss thresholds, and use them to study C−X bonds and the thermochemistry of monohalogenated cyclohexanes.

Carbon−halogen bonds are relevant and their energetics is important because of efforts to form them catalytically and relax the harsh reaction conditions required now[24] and to understand the halogen bond between electrophilic halogen-containing and nucleophilic moieties of a molecule.[25] PEPICO was in fact also used to confirm the role of radical chemistry in catalytic upgrading of natural gas by oxyhalogenation.[26,27] Furthermore, accurate thermochemical data for heavier halogen-containing species are few and far between.[28] This leads to a lack of test data to benchmark theoretical methods. As we will show here, standard density functional theory (DFT) approaches have been found to deliver accurate isodesmic reaction energies, but the accuracy of the G4 composite method for bromocyclohexane leaves much to be desired.

2. EXPERIMENTAL AND COMPUTATIONAL METHODS

Double-imaging photoelectron photoion coincidence (i^2PEPICO) experiments were carried out on halogenated cyclohexane samples ($C_6H_{11}X$, X = Cl, Br, and I; from Sigma-Aldrich) using the CRF-PEPICO endstation at the VUV beamline of the Swiss Light Source, Paul Scherrer Institute. The setup has been described in detail elsewhere,[29,30] and only a brief overview is given here. VUV photons from a bending magnet were dispersed by a grazing incidence monochromator with a 600 lines/mm laminar grating with an energy resolution of 2 meV at 8 eV. Before entering the ionization chamber, the VUV photons were focused into a differentially pumped gas filter, filled with a mixture of argon and neon to suppress higher-order radiation above 15.7 eV. The absolute photon energy was calibrated using autoionization lines of argon in the first and second order.

Samples were seeded into the ionization chamber through a needle valve at room temperature. After the VUV beam intersects the effusive beam and ionizes the sample, the electrons and ions were extracted in opposite directions by a constant, 125 V cm^{-1}, electric field. Electrons and ions were detected by position-sensitive delay-line anode detectors (Roentdek DLD40), installed at the end of the respective flight tubes, in velocity map imaging and, for the ions, also under space focusing conditions. Threshold electrons with less than 2 meV kinetic energy are projected onto the central spot of the detector together with the contamination by kinetic energy electrons that are formed without an off-axis momentum component. The latter was subtracted based on the signal in a small ring around the center spot, as proposed by Sztáray and Baer.[31] As the electron TOF is negligible relative to the ion TOF, electron hits are used as the start signal for the ion TOF analysis.[32] Thanks to the long ion acceleration region, metastable fragmentation processes in the $10^3 < k/s^{-1} < 10^7$ range show up as broad TOF peaks, which can be used to determine the unimolecular rate constant as a function of energy. Fractional threshold ionization parent and daughter abundances are plotted in the breakdown diagram, which is modeled simultaneously with the time-of-flight distributions for metastable dissociations to obtain accurate 0 K appearance energies.

The statistical modeling approach was detailed previously,[19] and only key aspects are emphasized here. Parent ions may fragment when their internal energy, that is, the sum of the photon energy and the thermal energy of the neutral sample minus the adiabatic ionization energy and the electron kinetic energy (negligible in threshold photoionization), is equal to or higher than the dissociation barrier. If the parent ion is metastable close to the dissociative photoionization threshold, slow dissociation rate constants in the 10^3 to 10^7 s^{-1} range result in asymmetrical fragment ion peak shapes and can be obtained based on the ion optics parameters.[33] In a fast dissociation without other competing processes, the integral of the internal energy distribution above the barrier yields the abundance of the fragment ion. If the parent ion is metastable or if multiple fragmentation processes compete, the fractional abundance of fragment ions will be affected by kinetic or competitive shifts, respectively, the magnitude of which can be determined by calculating the dissociation rate constants according to RRKM theory as[34−36]

$$k(E) = \frac{\sigma \cdot N^{\ddagger}(E - E_0)}{h \cdot \rho(E)} \quad (1)$$

where σ corresponds to the symmetry of the reaction coordinate, $N^{\ddagger}(E - E_0)$ is the number of states of the transition state at the excess energy, $E - E_0$, above the dissociation barrier, E_0 is the 0 K appearance energy, h is Planck's constant, and $\rho(E)$ is the density of states of the dissociating ion. The appearance energy is fitted, and the vibrational frequencies of the transitional modes in the transition state are scaled by a common factor to reproduce the experimental rate curve. In sequential dissociation processes, the internal energy distribution of the fragment ion is obtained by partitioning the excess energy statistically among the internal degrees of freedom of the fragment ion, the

https://dx.doi.org/10.1021/acs.jpca.0c10386
J. Phys. Chem. A 2021, 125, 646−656

neutral fragment, and the newly formed translations, without adjustable parameters.

Computed vibrational frequencies, rotational constants, and appearance energies are used to construct the initial statistical model. To provide this input, reactants, products, intermediates, and transition states were located on the $C_6H_{11}X^+$ ground-state potential energy surface using density functional theory at the B3LYP/6-311+G(d,p) level. Gaussian-4 (G4) theory[37] is not defined for iodine, and spin−orbit coupling means that the results for open-shell bromine-containing species may also be off by hundreds of meV.[38] Therefore, energies of the stationary points of species with only lighter atoms were further refined using G4 using the Gaussian 16 A.03 program package.[39] W1, CBS-QB3, and CBS-APNO calculations were carried out to support thermochemical derivations.[40,41] Isodesmic reaction energy calculations were also carried out using different DFT functionals and basis sets, including effective core potentials for X = Br and I. Further details are given in the Thermochemistry and Energetics section below. Basis sets and effective core potentials have in part been obtained from the Basis Set Exchange.[42]

3. RESULTS AND DISCUSSION

3.1. Threshold Ionization Mass Spectra and Breakdown Diagrams. Threshold photoionization TOF distributions were recorded in the 9.9−13.7, 9.6−15.0, and 8.9−15.0 eV photon energy range for $C_6H_{11}Cl$ (m/z 118 and 120, 3:1), $C_6H_{11}Br$ (m/z 162 and 164, 1:1), and $C_6H_{11}I$ (m/z 210), respectively. Representative threshold ionization mass spectra are shown in Figure 1. Asymmetric fragment ion peaks are seen in all three samples, namely, m/z 67 at 11.10 eV for Cl and m/z 55 at 12.90, 12.26 eV, and 11.51 eV for Cl, Br, and I, respectively. These are indicative of fragment ion formation in the acceleration region of the mass spectrometer, that is, of a metastable precursor ion and will be modeled quantitatively to account for the kinetic shift. Only this rate information and the threshold ionization cross section (proportional to the TPES) are lost when the threshold ionization mass spectra are reduced by plotting the fractional ion abundances as a function of photon energy in the breakdown diagram (Figure 2). The TPES is plotted in the background in Figure 2[17] because it can reveal if the dissociation mechanism is nonstatistical. The statistical model assumes that the ergodic hypothesis holds and the system can explore the whole phase space prior to dissociation. When the coupling between the electronic states is weak or the fragmentation is fast, isolated state behavior can arise, that is, the fragmentation mechanism of an electronic state will be decoupled from the rest.[43,44] Such states are normally isolated in energy as well, and isolated state behavior gives rise to a correlation between the breakdown diagram and the TPES.[45,46] The absence of such a correlation indicates that statistical theory can be reliably applied to the dissociative ionization of halocyclohexanes. If the coupling between the electronic states is strong, the phase space volume and, thus, the density of states of the dissociating ion are dominated by the lowest-energy, ground electronic state, and the ground state potential energy surface drives the fragmentation. This also implies conformational equilibrium, that is, axial and equatorial conformers can interconvert freely. As reported in the literature[11] and confirmed by our preliminary calculations, the interconversion rate between the two is on the order of 10^5 s^{-1} already at room temperature, implying well merging below the fragmentation threshold in the cation, as well. Therefore,

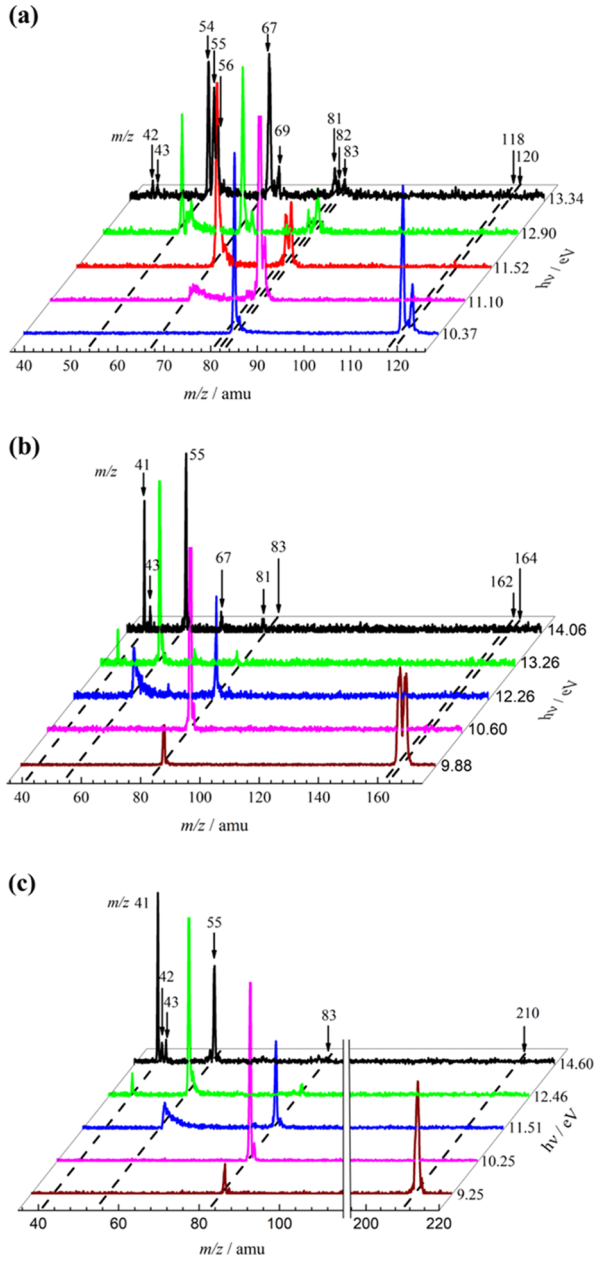

Figure 1. Threshold photoionization mass spectra of (a) $C_6H_{11}Cl$, (b) $C_6H_{11}Br$, and (c) $C_6H_{11}I$ at representative photon energies.

we only address the lowest-lying transition states and will show the equatorial cation isomer as the parent ion hereafter.

The parent ion fractional abundance is 100% at the ionization onset in the three samples, meaning that the potential energy well of the cation is deep enough to support the room temperature internal energy distribution of the sample at the ionization onset.[47] As the energy is increased, the parent peak loses intensity and different fragment ion peaks are observed depending on the halogen substituent.

In chlorocyclohexane, peaks at m/z 83, 82, 81, 69, 67, 56, 55, 54, 43, 42, and 41 showed up distinctly below 14 eV photon energy (Figure 1a). Among these, m/z 82 corresponds to HCl loss and is the most intense at lower energies. In contrast to fluorocyclohexane,[16] halogen atom loss also shows up at m/z 83 at higher energies, although it is never as important as in the heavier halocyclohexanes (*vide infra*). The

https://dx.doi.org/10.1021/acs.jpca.0c10386
J. Phys. Chem. A 2021, 125, 646−656

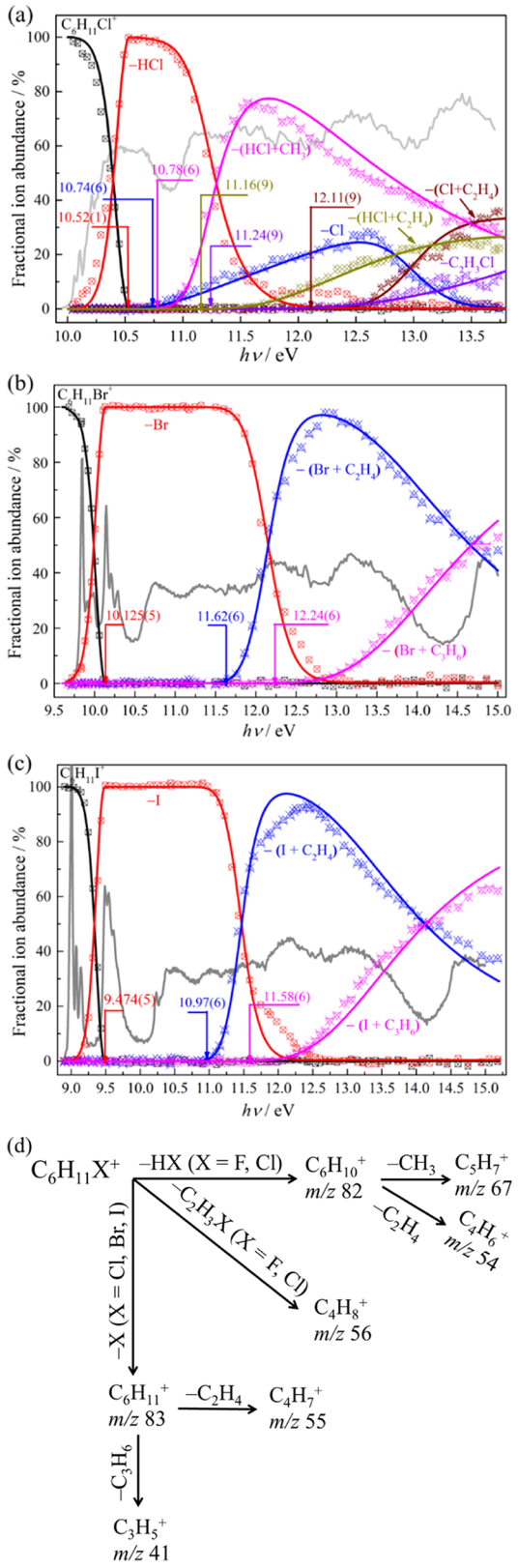

Figure 2. Breakdown diagram of (a) $C_6H_{11}Cl$, (b) $C_6H_{11}Br$, and (c) $C_6H_{11}I$. Crosses represent experimental fractional abundances, and the solid lines show the simulated results with the statistical model. The 0 K appearance energies of the major fragment ions were determined and noted with arrows. Solid gray lines correspond to the TPES. (d) Summary of the fragmentation mechanism as a function of the halogen substituent.

two peaks are not baseline-separated (Figure 1a), and the center of gravity of the m/z 82−83 band was used to apportion the ion signal to the HCl- and Cl-loss channels.[48] Above 12.9 eV, the m/z 56, 55, and 54 fragments appear with considerable intensity. Additional fragment ions at m/z 81, 69, 43, 42, and 41, seen at even higher energies with less than 10% abundance, are omitted in the breakdown diagram in Figure 2a. Of these, m/z 81 may be produced by H loss from m/z 82 and the m/z 69 fragment ion may be produced by the loss of CH_2Cl from the parent $C_6H_{11}Cl^+$ ion. The C_3 fragment ion cluster at m/z 41−43 is too weak to propose a plausible dissociation mechanism, but m/z 41 may be a sequential dissociation product of Cl loss (see below).

There is a continuous change in the dominant fragmentation pathways from fluorocyclohexane[16] to chloro-, bromo-, and iodocyclohexane cations. Thanks to the drop in H−X and C−X bond energies, the HX-loss channel is suppressed in X = Br and I, and the sole low-energy channel is halogen atom loss. At *ca.* 1.5 eV above the halogen atom loss threshold, the $C_4H_7^+$ fragment ion signal increases at m/z 55 with a highly asymmetric TOF profile at low energies. Since the parent ion is never metastable, the precursor to $C_4H_7^+$ must be the X-loss $C_6H_{11}^+$ cation. At even higher energies, the third dominant fragment channel, $C_3H_5^+$, starts increasing at m/z 41. Minor dissociative photoionization products are seen at m/z 81, 67, 43, and 42 with less than 10% abundance for X = Br and at m/z 43 and 42 for X = I. Their abundance is insufficient to propose a dissociation mechanism, and these channels are not plotted in the breakdown diagrams in Figure 2b,c.

To summarize, the DPI of $C_6H_{11}Cl$ exhibits a combination of features of fluorocyclohexane[16] and of the heavier analogues $C_6H_{11}Br$ and $C_6H_{11}I$. We can identify the parallel Cl-loss (m/z 83), HCl-loss (m/z 82), and C_2H_3Cl-loss (m/z 56) channels from the parent ion $C_6H_{11}Cl^+$, as well as the m/z 55 sequential fragmentation product from m/z 83 by C_2H_4 loss (similar to X = Br and I), while the m/z 67 and 54 ions are a sequential dissociation fragment from m/z 82 by CH_3 and C_2H_4 loss (similar to X = F), respectively. The fragmentation mechanism of $C_6H_{11}X^+$ (X = F, Cl, Br, and I) is summarized in Figure 2d.

The breakdown diagram offers valuable clues regarding the dissociation mechanism.[49] However, only a synergic approach between experiment, statistical modeling, and potential energy surface exploration can unleash the full potential of PEPICO.[50] In a recent study, the dissociative photoionization mechanism of 1,3-dioxolane was revealed including six chemically different fragmentation channels that lead to only three fragment ion m/z peaks.[51] While the experimental data may present an underdetermined problem in such a case, it was still possible to establish a credible mechanism by formulating a statistical model consistent with both the experimental data and the computed energetics. Therefore, we explored the viable and energetically allowed potential energy surface of the parent and intermediate halocyclohexane fragment ions, as guided by the experimental data, using constrained optimizations scanning bond lengths and angles, and refined the reaction energetics using composite methods when applicable.

3.2. Dissociation Pathways of $C_6H_{11}Cl^+$. Although the parent ion disappears from the breakdown diagram within 0.5 eV of the ionization energy, that is, the potential energy well of the parent ion is relatively shallow and the density of states is low at the fragmentation threshold, the HCl-loss daughter ion peak exhibits a slight asymmetry at its onset (see $h\nu$ = 10.37 eV in Figure 1a). This indicates low activation entropy, similar to

https://dx.doi.org/10.1021/acs.jpca.0c10386
J. Phys. Chem. A 2021, 125, 646−656

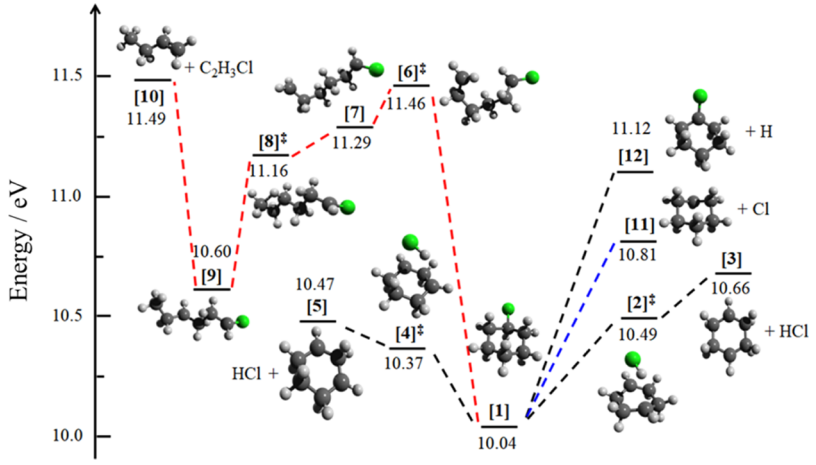

Figure 3. Reaction energetics of the initial fragmentation pathways of the chlorocyclohexane cation to yield the fragment ions at m/z 83, 82, and 56, as well as of the direct C−H bond fission. Energies are relative to the neutral equatorial $C_6H_{11}Cl$ and evaluated with the G4 composite method.

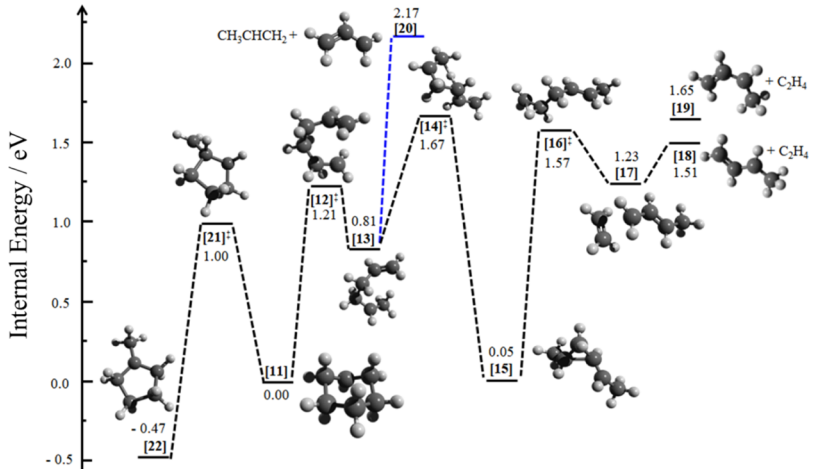

Figure 4. Dissociation pathways of the cyclohexyl ion to produce the fragment ions at m/z 55 and 41. The energies of intermediates and transition states are calculated using the G4 composite method, relative to the m/z 83 ion [**11**].

the dominant low-energy HF-loss channel in $C_6H_{11}F$.[16] Chlorocyclohexane is the lightest sample in the halocyclohexane series, in the dissociative ionization of which halogen atom loss is also observed, albeit as a minor channel. The m/z 83 fragment, seen only above 10.7 eV photon energy, corresponds to direct Cl loss, a parallel process to HCl loss. Halogen atom loss is, thus, a higher energy channel with a looser transition state and, therefore, more steeply increasing fragmentation rate constant with energy. At the same energy as the direct C−Cl bond breaking channel, the $C_5H_7^+$ fragment ion peak also increases at m/z 67. However, as seen at $h\nu$ = 11.10 eV in Figure 1a, it exhibits a highly asymmetric TOF profile at the onset. This implies that its precursor is metastable, which, in this case, can only be the HCl-loss fragment ion at m/z 82. Thus, m/z 67 is the CH_3-loss fragment ion of the HCl-loss intermediate.

We rely on the fluorocyclohexane results when exploring the $C_6H_{11}Cl^+$ dissociation channels leading to the shared m/z 82, 56, 67, and 54 fragment ions.[16] The m/z 82 and 56 fragment ions are the result of HCl and C_2H_3Cl losses from the parent ion. As will be discussed later, C_2H_3Cl loss is preceded by isomerization steps. As the isomeric identity of the HCl-loss $C_6H_{10}^+$ fragment ion at m/z 82 is fluid, its sequential fragmentation steps to m/z 67 and 54 are the same as those of the HF-loss fragment ion of fluorocyclohexane.

The G4-calculated fragmentation pathways from the $C_6H_{11}Cl^+$ cation leading to the m/z 83, 82, and 56 ions are displayed in Figure 3, together with the unobserved direct C−H bond fission channel leading to [**12**] shown for completeness. In the lowest energy fragmentation channel to $C_6H_{10}^+$ + HCl at 0.43 eV, Cl forms a bond with a H from the *meta* position [**5**] *via* the transition state [**4**]‡ at 0.33 eV. Note that the G4-computed product energy is higher than the transition state energy for [**5**] and [**4**],‡ as well as for [**3**] and [**2**]‡. This is due to a discrepancy between the density functional theory and the more expensive wave function theory potential energy surfaces, which are used in G4 to determine the geometry and the energy at the geometry, respectively.[37,52] Because G4 involves up to CCSD(T) coupled cluster wave function theory calculations, we are inclined to assume that the computed energetics represents the potential energy landscape quite well. This suggests that HCl may be lost along a purely attractive reaction energy curve or a submerged transition state. The analogous HF loss in $C_6H_{11}F^+$ is kinetically controlled, and a H atom from the *para* position is extracted to yield the more energetic fragment ion [**3**]. With respect to the parent ion, [**3**] lies at 0.62 eV, that is, *ca.* 0.2 eV higher than

https://dx.doi.org/10.1021/acs.jpca.0c10386
J. Phys. Chem. A 2021, 125, 646−656

[5], and can also be produced by HCl loss without a reverse barrier, that is, the dissociative photoionization threshold is determined by the product energetics. The isomerization path connecting these two HX-loss products and further sequential dissociation pathways from m/z 82 to m/z 67 and 54 have already been discussed in detail for $C_6H_{11}F^+$.[16]

The lowest energy C_2H_3Cl-loss pathway from $C_6H_{11}Cl^+$ to the m/z 56 fragment is also analogous with the C_2H_3F-loss pathway in $C_6H_{11}F^+$.[16] First, the C1−C6 bond is broken over transition state [**6**]‡ at 11.46 eV, followed by ring-opening to [**7**] at 11.29 eV. DFT geometry optimization predicts transition state [**8**]‡ for the H-transfer from C4 to the terminal carbon atom C6 in [**9**] at 10.60 eV, but the process is downhill according to G4 energies. Finally, the C2−C3 bond is broken and C_2H_3Cl is released at 11.49 eV to yield the 1-butene cation at m/z 56 [**10**]. Here again, the product energies are the highest, although by a smaller margin than in HCl loss, which suggest that the dissociative ionization threshold may correspond to the reaction energy.

The C−Cl bond energy was calculated at 0.77 eV in the chlorocyclohexane cation, much less than the C−F bond breaking energy of 1.90 eV in $C_6H_{11}F^+$. This explains the appearance of the halogen-atom-loss fragment ion at m/z 83. Sequential channels from m/z 83 to m/z 55 and 41 are the dominant channels in bromo- and iodocyclohexane and will be discussed there.

3.3. Dissociation Pathways of $C_6H_{11}Br^+$ and $C_6H_{11}I^+$. Because of the declining C−X and X−H bond energies as a function of halogen atom size, the threshold to hydrogen halogenide loss increases, while that to halogen atom loss drops precipitously in the halocyclohexane series.[15] As a result, the first and dominant dissociation channel is the loss of the halogen atom, yielding the m/z 83 fragment, [**11**], in both $C_6H_{11}Br^+$ and $C_6H_{11}I^+$. DFT scans suggest that halogen loss takes place without a reverse barrier. Figure 4 only shows the mutual DPI pathways after halogen loss, that is, the dissociation pathway of the cyclohexyl cation.

Both energetic arguments and the slope of the breakdown curves suggest that the m/z 55 [**18**] and 41 [**20**] fragment ions are formed in consecutive dissociation steps of the X-loss fragment ion at m/z 83 [**11**] from X = Br and I. In the reaction pathways shown in Figure 4, the energy is referenced to the cyclohexyl cation [**11**]. The first sequential fragment of m/z 83 is the m/z 55 fragment ion, [**18**], by ethylene loss (28 amu). In a ring-opening step, a hydrogen atom is transferred from C4 to C3 over transition state [**12**]‡ at 1.21 eV. The resulting intermediate [**13**] at 0.81 eV undergoes H-transfer from C5 to C2 over a five-membered ring transition state [**14**]‡ at 1.67 eV. The intermediate state [**15**] contains a three-membered ring and is only 0.05 eV less stable than the cyclohexyl cation. A hydrogen transfer from the CH_3 group, which is attached to the three-membered ring, to an adjacent carbon over transition state [**16**]‡ at 1.57 eV yields the next intermediate [**17**] at 1.23 eV. This can lose C_2H_4 directly to yield the *trans*-1-methylallyl cation [**18**] at 1.51 eV.[53] For completeness, the more energetic *cis*-1-methylallyl cation [**19**] is also shown at 1.65 eV, which can be produced *via* the transfer of the other C5 hydrogen. In $C_6H_{11}Br$ and $C_6H_{11}I$, the m/z 55 and 41 breakdown curves in Figure 2b,c exhibit a broad crossover region and slowly changing abundances, which correspond to slowly changing rate constant ratios and, hence, to competing fragmentation channels. Indeed, the 3-propenyl fragment ion [**20**] at m/z 41 can be produced from the intermediate [**13**] by direct bond fission, yielding the CH_3CHCH_2 neutral fragment at an energy of 2.17 eV.

It is important to note that the cyclohexyl cation can also ring-contract to the more stable methylcyclopentyl [**22**] cation over transition state [**21**]‡ at 1.00 eV. In fact, hydride abstraction from cyclohexane is known to yield the 1-methylcyclopentyl cation,[54] and the product ion was indistinguishable from 1-methylcyclopentyl in cyclohexene protonation experiments too.[55] This suggests that isomerization will also readily take place under our experimental conditions. However, our calculations indicate that the lowest energy fragmentation pathways from the methylcyclopentene cation all start from the cyclohexyl structure, as plotted in Figure 4.

3.4. Unimolecular Dissociation Model. Based on the calculated reaction paths, we set up a statistical model to reproduce the experimental breakdown diagram and asymmetric daughter ion peaks.[19] In $C_6H_{11}Cl$, the lowest-energy decomposition channel is the loss of HCl molecules, and the 0 K appearance energy (E_0) of the m/z 82 ion is determined as 10.52 ± 0.01 eV (Figure 2a). This value is consistent with the calculated DPI threshold to [**5**] at 10.47 eV. The model $E_0(C_6H_{11}^+/C_6H_{11}Cl)$ for Cl loss is affected by a competitive shift, that is, the breakdown curve is indicative of the relative rate constants and requires extrapolation to the threshold. The experimental value, 10.74 ± 0.06 eV, still agrees reasonably well with the calculated result of 10.81 eV to [**11**]. The competitive shift affects the next parallel fragment channel, m/z 56, much more, and the breakdown curve increases slowly near threshold. The model result suggests a competitive shift in excess of 1 eV at $E_0(C_4H_8^+)$ = 11.24 ± 0.09 eV. The fitted appearance energy is significantly lower than the calculated value of 11.49 eV to [**10**]. A possible reason for this deviation is that the HCl-loss rate constant increases less steeply at high energies than predicted by the statistical model, and the model overestimates the competitive shift.

Sequential CH_3 loss and C_2H_4 loss from m/z 82 lead to the m/z 67 and 54 product ions, respectively. Similar to the case of HF loss in the DPI of fluorocyclohexane, the HCl-loss product at m/z 82 will undergo significant stabilization: the cyclohexene and 1-methylcyclopentene cations are 0.83 and 1.18 eV more stable than the prompt fragment ion by *meta*-H elimination (see Figure 5 in ref 16). Thus, the effective potential energy well of the m/z 82 cation is deep, which leads to a large density of states at the sequential fragmentation thresholds. Taking this into account to model the kinetic shift, similarly to the fluorocyclohexane analogue, explains the slow dissociation rate constants despite the small energy gap between the HCl and sequential methyl loss onsets and yields a fitted $E_0(C_5H_7^+/C_6H_{11}Cl)$ of 10.78 ± 0.06 eV and $E_0(C_4H_6^+/C_6H_{11}Cl)$ of 11.16 ± 0.09 eV (Figure 2a). These values are 0.26 and 0.64 eV higher, respectively, than the HCl-loss threshold at 10.52 ± 0.01 eV. They can be compared with a previously computed potential energy of the m/z 82 cation, in which the m/z 67 and 54 sequential dissociation thresholds were found to be 0.45 and 0.95 eV above the prompt HCl-loss product ion at m/z 82, respectively.[16] A small fraction of the m/z 82 signal persists at high photon energies, which may indicate that HCl loss may also proceed over a sizeable reverse barrier, forming a stabilized fragment ion directly, after which the kinetic energy release decreases the internal energy of the m/z 82 fragment available for consecutive dissociation steps.

https://dx.doi.org/10.1021/acs.jpca.0c10386
J. Phys. Chem. A 2021, 125, 646−656

The primary halogen-loss fragment at m/z 83 ($C_6H_{11}^+$) yields m/z 55 and m/z 41 ions in consecutive ethene and propene losses, respectively. In the energy range of the X = Cl breakdown diagram, only m/z 55 was observed at a threshold energy of $E_0(C_4H_7^+/C_6H_{11}Cl)$ = 12.11 ± 0.09 eV. This implies a $E_0(C_4H_7^+/C_6H_{11}Cl) - E_0(C_6H_{11}^+/C_6H_{11}Cl)$ = 1.37 eV barrier to ethene loss from $C_6H_{11}^+$, which is also lower than the 1.50 eV barrier deduced from the statistical model to the DPI of bromo- and iodocyclohexane (*vide infra*) and a G4-computed activation energy of 1.67 eV ([**11**] → [**14**]‡ → [**18**] in Figure 4).

As discussed previously, only halogen atom loss was observed in the primary DPI of $C_6H_{11}Br$ and $C_6H_{11}I$, and thus, the consecutive dissociation channels are shared. The 0 K appearance energies for C−Br or C−I bond breaking are determined experimentally as $E_0(C_6H_{11}^+/C_6H_{11}Br)$ = 10.125 ± 0.005 eV (Figure 2b) and $E_0(C_6H_{11}^+/C_6H_{11}I)$ = 9.474 ± 0.005 eV (Figure 2c), respectively. The fitted 0 K appearance energies for the two sequential dissociation channels m/z 55 and 41, that is, ethene and propene loss, are $E_0(C_4H_7^+/C_6H_{11}Br)$ = 11.62 ± 0.06 eV and $E_0(C_3H_5^+/C_6H_{11}Br)$ = 12.24 ± 0.06 eV for $C_6H_{11}Br$, as well as $E_0(C_4H_7^+/C_6H_{11}I)$ = 10.97 ± 0.06 eV and $E_0(C_3H_5^+/C_6H_{11}Br)$ = 11.58 ± 0.06 eV for $C_6H_{11}I$. Thus, the barrier to the m/z 55 and 41 fragments from the cyclohexyl cation at m/z 83 is 1.50 and 2.12 eV, respectively, based on the statistical model for $C_6H_{11}Br$, as well as 1.50 and 2.11 eV, respectively, based on the $C_6H_{11}I$ data. These results are also in agreement with the quantum chemical calculations, which yield 1.67 and 2.17 eV, respectively ([**11**] → [**14**]‡ → [**18**] and [**11**] → [**20**] in Figure 4). We can also observe that the m/z 83 signal is underestimated by the model close to its disappearance. Similar to the HCl-loss breakdown curve in chlorocyclohexane, the reason could be that a more stable $C_6H_{11}^+$ isomer, that is, the methylcyclopentyl cation is formed over a reverse barrier, which entails excess kinetic energy release, thereby reducing the m/z 83 fragment ion internal energy and stabilizing it. However, the effect is not observed in Cl, small in Br, and more pronounced in I. Thus, an alternative explanation is that the less stable $^2P_{1/2}$ halogen atoms are also formed besides the $^2P_{3/2}$ spin−orbit state. This could account for 0.11, 0.46, and 0.94 eV less internal energy in the fragment ion,[38,56,57] explaining the increasing persistence of the m/z 83 signal in the Cl < Br < I series, respectively.

3.5. Thermochemistry and Energetics. Appearance energies in chloro-, bromo-, and iodocyclohexane correspond to product energies and may be used in ion cycle calculations.

As far as X = Cl is concerned, the lowest-energy HCl-loss threshold is confounding, partly because H-abstraction from the *meta* position yields a metastable fragment, which may then isomerize to the cyclohexene or the methylcyclopentene cation, and partly because the stability of the m/z 83 ion is markedly smaller experimentally than predicted computationally.

Direct C−Cl bond fission yields the cyclohexyl cation, that is, protonated cyclohexene at E_0 = 10.74 ± 0.06 eV = 1036.2 ± 5.8 kJ mol^{-1}. The proton affinity (PA) of cyclohexene was reported relative to that of acetone by Lias *et al.*,[55] which converts to PA(c-C_6H_{10}) = 783 ± 14 kJ mol^{-1} using the revised acetone PA by Hunter and Lias.[58] Hunter and Lias also re-evaluated the PA(c-C_6H_{10}) and list it as 784.5 kJ mol^{-1}. The cyclohexene enthalpy of formation was measured very carefully by Steele *et al.* using (rotating) bomb calorimetry both by combustion and by hydrogenation as $\Delta_fH^o_{298K}$(c-C_6H_{10}, g) = −4.32 ± 0.98 kJ mol^{-1}.[59] This converts to 27.2 ± 1 kJ mol^{-1} at 0 K using the G4-computed thermal enthalpy of gaseous cyclohexene (17.2 kJ mol^{-1}) and the standard elemental thermal enthalpies.[60] The G4-, CBS-QB3-, CBS-APNO-, and W1-calculated 0 K proton affinity of cyclohexene can be averaged to 766.7 ± 1.7 kJ mol^{-1} using double the standard deviation as uncertainty, which can be converted to 771.5 kJ mol^{-1} at 298 K. The cyclohexene enthalpy of formation, the cyclohexene proton affinity, and the 0 K heat of formation[28] of H^+ of 1528.08 kJ mol^{-1} thus yield $\Delta_fH^o_{0K}$(c-$C_6H_{11}^+$) = 788.5 ± 2.2 kJ mol^{-1}. Together with $\Delta_fH^o_{0K}$(Cl) = 119.62 kJ mol^{-1}, as reported by the Active Thermochemical Tables (ATcT), and $E_0(C_6H_{11}^+/C_6H_{11}Cl)$ = 1036.2 ± 5.8 kJ mol^{-1}, this yields $\Delta_fH^o_{0K}$($C_6H_{11}Cl$, g) = −128.1 ± 6.2 kJ mol^{-1}, which, using the elemental thermal enthalpies and a G4-computed thermal enthalpy of 21.1 kJ mol^{-1}, converts to −164.4 ± 6.2 kJ mol^{-1} at 298 K. This value includes the 0.5 kJ mol^{-1} effect of the conformational equilibrium on the thermal enthalpy (see below).

For comparison, the most recent experimental value has been reported at −166.5 ± 1.9 kJ mol^{-1}.[61] We have also evaluated the 0 K isodesmic reaction energies of

$$CH_3Cl + C_6H_{12} \rightarrow C_6H_{11}Cl + CH_4 \quad (2)$$

and

$$C_2H_5Cl + C_6H_{12} \rightarrow C_6H_{11}Cl + C_2H_6 \quad (3)$$

using the 0 K (chloro)alkane heats of formation, as listed in the ATcT. The heat of formation of liquid cyclohexane was reported as −156.1 ± 0.7 kJ mol^{-1},[62] which, together with an enthalpy of vaporization of 32.98 ± 0.02 kJ mol^{-1},[63] yields −123.2 ± 0.7 kJ mol^{-1} at 298 K, and, using a G4 thermal enthalpy of 17.7 kJ mol^{-1}, $\Delta_fH^o_{0K}$(c-C_6H_{12}, g) = −83.8 ± 0.7 kJ mol^{-1} at 0 K. The G4, CBS-QB3, and W1 isodesmic reaction energies could be used to derive $\Delta_fH^o_{0K}$(c-$C_6H_{11}Cl$, g) = −131.8 ± 3.3 kJ mol^{-1}, which converts to $\Delta_fH^o_{298K}$(c-$C_6H_{11}Cl$, g) = −168.6 ± 3.3 kJ mol^{-1}. Thus, the DPI modeling result and the isodesmic reaction energy calculations both confirm the previous literature value but are less accurate. The uncertainty in the experimental result is due to the competitive shift, since Cl loss is not the lowest-energy channel.

The cyclohexyl cation ($\Delta_fH^o_{0K}$(c-$C_6H_{11}^+$) = 788.5 ± 2.2 kJ mol^{-1}, see above) is also the product of halogen atom loss by direct bond cleavage in the DPI of bromo- and iodocyclohexane. The modeled 0 K appearance energies are $E_0(C_6H_{11}^+/C_6H_{11}Br)$ = 10.125 ± 0.005 eV = 976.9 ± 0.5 kJ mol^{-1} and $E_0(C_6H_{11}^+/C_6H_{11}I)$ = 9.474 ± 0.005 eV = 914.1 ± 0.5 kJ mol^{-1}. Together with ATcT values of $\Delta_fH^o_{0K}$(Br (g)) = 117.91 ± 0.06 kJ mol^{-1} and $\Delta_fH^o_{0K}$(I (g)) = 107.157 ± 0.002 kJ mol^{-1}, we can derive $\Delta_fH^o_{0K}$($C_6H_{11}Br$ (g)) = −70.5 ± 2.3 kJ mol^{-1} and $\Delta_fH^o_{0K}$($C_6H_{11}I$ (g)) = −18.4 ± 2.3 kJ mol^{-1}. We calculated the 0 K energy of the axial conformer to be 2.2 and 2.1 kJ mol^{-1} higher than that of the equatorial one in X = Br and I, respectively, using ωB97X-D/(SDB-)cc-pVTZ. The thermal enthalpy of the axial conformer is 0.3 kJ mol^{-1} lower for both, which means that the conformational equilibrium increases the thermal enthalpy of the equatorial conformer by 0.6 kJ mol^{-1} for both X = Br and I. Adding this correction and using the elemental and the computed thermal enthalpies, these values can be converted to $\Delta_fH^o_{298K}$($C_6H_{11}Br$ (g)) = −114.4 ± 2.3 kJ mol^{-1} and $\Delta_fH^o_{298K}$($C_6H_{11}I$ (g)) = −56.3 ±

https://dx.doi.org/10.1021/acs.jpca.0c10386
J. Phys. Chem. A 2021, 125, 646−656

Table 1. Comparison of the Experimentally Derived and Calculated 0 K Enthalpies of Formation of Bromo- and Iodocyclohexane in kJ mol^{-1}[a]

method	comp. cost	$\Delta_f H°_{0K}(C_6H_{11}Br)$	$\Delta[(2)-(3)]$	Δ_{Br}[calc-expt]	$\Delta_f H°_{0K}(C_6H_{11}I)$	Δ_I[calc-expt]
expt.		−70.5 ± 2.3			−18.4 ± 2.3	
G4	4.8	−77.9	−1.7	−7.5		
CBS-QB3	1.0	−71.6	−0.3	−1.2		
ωB97X-D/(SDB-)cc-pVTZ	1.2 (1.6)	−70.0	1.8	0.4	−17.5	0.9
M06-2X-D3/aug-cc-pVTZ(-PP)	4.2 (5.1)	−71.7	0.6	−1.1	−19.7	−1.3
PBE/def2-TZVPP	1.0 (1.2)	−69.5	1.1	1.0	−17.4	1.0
B3LYP/6-311G(d,p)	0.1 (0.1)	−67.6	2.6	2.9	−13.9	4.5

[a]Average results for the two isodesmic reactions analogous to (2) and (3) are listed for X = Br with the difference given in the column $\Delta[(2)-(3)]$. Only the analogous isodesmic reaction to (2) was studied for X = I. The computational cost is based on the relative wall time of the PBE $C_6H_{11}Br$ calculation and is given in parentheses for the X = I calculations.

2.3 kJ mol^{-1}, which are the first reported enthalpies of formation for these species, to the best of our knowledge.

Isodesmic reaction energies were also calculated for the analogous reactions to (2) and to (3) for X = Br and to (2) for X = I. The 0 K enthalpies for the formation of gaseous CH_3Br, C_2H_5Br, and CH_3I are listed as −20.88 ± 0.18, −41.4 ± 0.25, and 24.5 ± 0.18 kJ mol^{-1} in ATcT, respectively. G4 and CBS-QB3 can be applied to X = Br, but none of the composite methods is defined for X = I. Therefore, we thought that it would be informative to apply widely used DFT approaches to both heavy halogen samples to check their performance against the experimental energetics. We used (1) the ωB97X-D functional[64] with the (SDB-)cc-pVTZ basis set including the 28- and 46-electron quasi-relativistic Stuttgart effective core potential on bromine and iodine, respectively,[65,66] as applied in studying iodine-loss kinetics in 1-iodoalkane cations;[20] (2) the M06-2X-D3 functional[67] including empirical dispersion interaction corrections,[68] with the aug-cc-pVTZ(-PP) basis set including 10- and 28-electron ECP on bromine and iodine,[69] as applied, for example, in the study of iodine catalysis;[70] and (3) the PBE functional[71,72] with the def2-TZVPP basis set, which includes a 28-electron ECP on iodine,[69,73] as applied in calculations on iodine-catalyzed benzylic C−H amination.[74] For comparison, we also include B3LYP/6-311G(d,p) results in the derived 0 K enthalpies of formation, listed together with the experimental ones in Table 1. G4 is more accurate than the best DFT approaches by at least a factor of two for reference sets mostly containing light molecules.[75] In contrast, G4 took almost five times longer than PBE/def2-TZVPP to deliver one of the least consistent and the least accurate result for $C_6H_{11}Br$, which surprised us. Checking the details, we found that the first step in the G4 recipe, the B3LYP geometry optimization (of which the electronic energy does not figure in the G4 electronic energy), outperforms the full G4 calculations at an average error of 1.7 kJ mol^{-1}. The computed CCSD(T) basis of the G4 energies, together with the zero-point correction, is in error by −4.8 kJ mol^{-1}. In G4, there are three corrections for basis set incompleteness in electron correlation calculations; these make the agreement worse by further −3.9 kJ mol^{-1}, which is only partly counteracted by the HF extrapolation improving the agreement by 1.2 kJ mol^{-1}. This is how the average −7.5 kJ mol^{-1} disagreement comes to be (see Table 1). Thus, there does not seem to be a single well-defined G4 computation step responsible for the discrepancy. The second insight, by which we were positively surprised, is that the other methods, at least beyond B3LYP/6-311G(d,p), delivered energetics within the uncertainty of the experiment. Thus, it appears that isodesmic reaction energy calculations provide a quite robust route for determining the energetics of closed-shell species containing even iodine.

With the help of the $C_6H_{11}X$ (X = Cl, Br, and I) ionization energies of 10.06, 9.71, and 8.99 eV[17] and the reported X-loss appearance energies herein, we can also obtain the C−X bond energy in the halocyclohexane cations as 66, 40, and 47 kJ mol^{-1}, respectively. The ionization of *eq*-$C_6H_{11}Br$ entails significant geometry relaxation to the ground pseudo-A″ cation state, which means that its ionization energy is not well defined. However, if we consider the sharp resonance at 9.85 eV (which was previously believed to correspond to the adiabatic ionization energy of the equatorial conformer),[76] the derived C−Br bond energy evaluates to 26 kJ mol^{-1} in the corresponding A′ cation state. This U-shaped trend is, however, only counterintuitive on the first sight. The atomic polar tensor (APT) charges[77] on the halogen in the halocyclohexane cations increase monotonically from −0.52 in X = F to 0.37 in X = I. On the one hand, the decreasing electrophilicity of the substituent stabilizes the ion and leads to a drop in ionization energy. When a neutral halogen is lost from the cation, the charge remains quantitatively on the cycloalkyl cation, which means that this stabilization effect is lost, increasing the bond energy in the halocyclohexane cations for heavier halogens. On the other hand, the C−X bond energy, corresponding to $C_6H_{11}X \rightarrow C_6H_{11}^{\bullet} + X^{\bullet}$, decreases in the F → I series in the neutral, a trend, which is faithfully reproduced by the X-loss appearance energy in DPI ($C_6H_{11}X \rightarrow C_6H_{11}^{+} + X^{\bullet} + e^{-}$), only shifted by the ionization energy of the cyclohexyl radical. The resultant of these two effects is that the C−X bond energy in the halocyclohexane cations is minimal for X = Br.

4. CONCLUSIONS

Halogen atom loss and sequential fragmentation of the cyclohexyl cation constitute the dissociative photoionization mechanism of bromo- and iodocyclohexane. In addition to Cl loss, chlorocyclohexane also exhibits the DPI mechanism previously observed in fluorocyclohexane, namely, HX loss followed by methyl and ethylene losses. Because HCl loss is the lowest-energy channel, Cl loss is affected by a competitive shift, increasing the uncertainty of the 0 K appearance energy. With the help of a statistical model, the X-loss E_0 in $C_6H_{11}X$ has been determined as 10.74 ± 0.06 eV, 10.125 ± 0.005, and 9.474 ± 0.005 eV for X = Cl, Br, and I, respectively. The appearance energies of the consecutive steps are also reported and compared with the computed potential energy surface. In particular, for X = Br and I, the good agreement between

https://dx.doi.org/10.1021/acs.jpca.0c10386
J. Phys. Chem. A 2021, 125, 646−656

experiment and theory for the consecutive steps strongly suggests that the initial DPI product is indeed the cyclohexyl cation, and it is from this fragment that further fragmentation steps start, notwithstanding possible isomerization to the more stable 1-methylcyclopentyl cation.

The proton affinity of cyclohexene was revised with the help of extensive calculations to $PA_{298K}(c\text{-}C_6H_{10})$ = 771.5 ± 1.7 kJ mol^{-1} and used in concert with literature thermochemical data to obtain the enthalpy of formation of the cyclohexyl cation as $\Delta_f H^\circ_{0K}(c\text{-}C_6H_{11}^+)$ = 788.5 ± 2.2 kJ mol^{-1}. This leads to an experimental $\Delta_f H^\circ_{298K}(C_6H_{11}Cl, g)$ = −164.4 ± 6.2 kJ mol^{-1}, which agrees with the result of isodesmic calculations (−168.6 ± 3.3 kJ mol^{-1}) and the literature value of −166.5 ± 1.9 kJ mol^{-1} but is less accurate than either.

The halogen-loss onset could be determined accurately in bromo- and iodocyclohexane, and we report their enthalpies of formation as $\Delta_f H^\circ_{298K}(C_6H_{11}Br, g)$ = −114.4 ± 2.3 kJ mol^{-1} and $\Delta_f H^\circ_{298K}(C_6H_{11}I, g)$ = −56.3 ± 2.3 kJ mol^{-1}, respectively. Halogen exchange isodesmic reaction energies were computed using various DFT approaches for X = Br and I, as well as using G4 and CBS-QB3 for X = Br. DFT approaches deliver surprisingly accurate results. G4, however, was found to be 50 times more time consuming yet still less accurate than B3LYP/6-311G(d,p) for bromocyclohexane.

Finally, we use the halocyclohexane ionization energies to determine the C−X bond energy in the $C_6H_{11}X^+$ cation and find the C−Br bond to be the weakest. This is due to the decreasing C−X bond energy in the neutral with increasing halogen size, which competes with the stabilization of the halocyclohexane cation when using less electrophilic, larger halogen substituents.

AUTHOR INFORMATION

Corresponding Authors

Xiaoguo Zhou − *Hefei National Laboratory for Physical Sciences at the Microscale, Department of Chemical Physics, University of Science and Technology of China, Hefei 230026, China;* orcid.org/0000-0002-0264-0146; Email: xzhou@ustc.edu.cn

Andras Bodi − *Paul Scherrer Institute, Villigen 5232, Switzerland;* orcid.org/0000-0003-2742-1051; Email: andras.boedi@psi.ch

Authors

Xiangkun Wu − *Paul Scherrer Institute, Villigen 5232, Switzerland; Hefei National Laboratory for Physical Sciences at the Microscale, Department of Chemical Physics, University of Science and Technology of China, Hefei 230026, China;* orcid.org/0000-0001-8515-3302

Patrick Hemberger − *Paul Scherrer Institute, Villigen 5232, Switzerland*

Complete contact information is available at: https://pubs.acs.org/10.1021/acs.jpca.0c10386

Notes

The authors declare no competing financial interest.

ACKNOWLEDGMENTS

The experiments were carried out at the VUV beamline of the Swiss Light Source of the Paul Scherrer Institute. The financial support of the Swiss Federal Office for Energy (BFE contract no. SI/501269-01) and the National Natural Science Foundation of China (nos. 21903079 and 21873089) is gratefully acknowledged. The work was also financially supported by the National Key Research and Development Program of China (no. 2016YFF0200502). X.W. thanks the SSSTC scholarship (grant no. EG-CN 01-042018), the China Scholarship Council (grant no. 201806340001), and the USTC-NSRL for support.

REFERENCES

(1) Baer, T.; Tuckett, R. P. Advances in threshold photoelectron spectroscopy (TPES) and threshold photoelectron photoion coincidence (TPEPICO). *Phys. Chem. Chem. Phys.* **2017**, *19*, 9698−9723.

(2) Bodi, A.; Hemberger, P.; Osborn, D. L.; Sztáray, B. Mass-resolved isomer-selective chemical analysis with imaging photoelectron photoion coincidence spectroscopy. *J. Phys. Chem. Lett.* **2013**, *4*, 2948−2952.

(3) McCabe, M. N.; Hemberger, P.; Reusch, E.; Bodi, A.; Bouwman, J. Off the Beaten Path: Almost Clean Formation of Indene from the ortho-Benzyne + Allyl Reaction. *J. Phys. Chem. Lett.* **2020**, *11*, 2859−2863.

(4) Hemberger, P.; Custodis, V. B.; Bodi, A.; Gerber, T.; van Bokhoven, J. A. Understanding the mechanism of catalytic fast pyrolysis by unveiling reactive intermediates in heterogeneous catalysis. *Nat. Commun.* **2017**, *8*, 15946.

(5) Hemberger, P.; van Bokhoven, J. A.; Pérez-Ramírez, J.; Bodi, A. New analytical tools for advanced mechanistic studies in catalysis: Photoionization and photoelectron photoion coincidence spectroscopy. *Catal. Sci. Technol.* **2020**, *10*, 1975−1990.

(6) Park, S. T.; Kim, S. K.; Kim, M. S. Observation of conformation-specific pathways in the photodissociation of 1-iodopropane ions. *Nature* **2002**, *415*, 306.

(7) Kim, M. H.; Shen, L.; Tao, H.; Martinez, T. J.; Suits, A. G. Conformationally controlled chemistry: Excited-state dynamics dictate ground-state reaction. *Science* **2007**, *315*, 1561−1565.

(8) Lim, J. S.; Lee, Y. S.; Kim, S. K. Control of intramolecular orbital alignment in the photodissociation of thiophenol: Conformational manipulation by chemical substitution. *Angew. Chem., Int. Ed.* **2008**, *47*, 1853−1856.

(9) Choi, K.-W.; Ahn, D.-S.; Lee, J.-H.; Kim, S. K. A highly conformationally specific α- and β-Ala+decarboxylation pathway. *Chem. Commun.* **2007**, 1041−1043.

(10) McMurry, J. *Organic Chemistry*; Thomson-Brooks/Cole: Belmont, 2004.

(11) Jensen, F. R.; Bushweller, C. H. Separation of conformers. II. Axial and equatorial isomers of chlorocyclohexane and trideuteriomethoxycyclohexane. *J. Am. Chem. Soc.* **1969**, *91*, 3223−3225.

(12) Ribeiro, D. S.; Rittner, R. The role of hyperconjugation in the conformational analysis of methylcyclohexane and methylheterocyclohexanes. *J. Org. Chem.* **2003**, *68*, 6780−6787.

(13) Bodi, A.; Bjornsson, R.; Arnason, I. A phenomenological relationship between molecular geometry change and conformational energy change. *J. Mol. Struct.* **2010**, *978*, 14−19.

(14) Bjornsson, R.; Arnason, I. Conformational properties of six-membered heterocycles: Accurate relative energy differences with dft, the importance of dispersion interactions and silicon substitution effects. *Phys. Chem. Chem. Phys.* **2009**, *11*, 8689−8697.

(15) Bodi, A.; Sigurdardottir, K. L.; Kvaran, Á.; Bjornsson, R.; Arnason, I. Dissociative photoionization of 1-halogenated silacyclohexanes: Silicon traps the halogen. *J. Phys. Chem. A* **2016**, *120*, 9188−9197.

(16) Wu, X.; Zhou, X.; Hemberger, P.; Bodi, A. A guinea pig for conformer selectivity and mechanistic insights into dissociative ionization by photoelectron photoion coincidence: Fluorocyclohexane. *Phys. Chem. Chem. Phys.* **2020**, *22*, 2351.

(17) Wu, X.; Zhou, X.; Hemberger, P.; Bodi, A. Conformers, electronic states, and diabolical conical intersections in the valence photoelectron spectroscopy of halocyclohexanes. *J. Chem. Phys.* **2020**, *153*, 054305.

(18) Wu, X.-k.; Tang, X.-f.; Zhou, X.-g.; Liu, S.-l. Dissociation dynamics of energy-selected ions using threshold photoelectron-photoion coincidence velocity imaging. *Chin. J. Chem. Phys.* **2019**, *32*, 11−22.
(19) Sztáray, B.; Bodi, A.; Baer, T. Modeling unimolecular reactions in photoelectron photoion coincidence experiments. *J. Mass Spectrom.* **2010**, *45*, 1233−1245.
(20) Rowland, T. G.; Borkar, S.; Bodi, A.; Sztáray, B. Iodine atom loss kinetics in internal energy selected 1-iodoalkane cations by imaging photoelectron photoion coincidence spectroscopy. *Int. J. Mass spectrom.* **2015**, *378*, 134−142.
(21) Bodi, A.; Hemberger, P. Imaging breakdown diagrams for bromobutyne isomers with photoelectron-photoion coincidence. *Phys. Chem. Chem. Phys.* **2014**, *16*, 505−515.
(22) Borkar, S.; Sztáray, B.; Bodi, A. Dissociating c3h5br+ ions: Almost all roads lead to the allyl cation. *Int. J. Mass spectrom.* **2012**, *330*−*332*, 100−108.
(23) Sergeev, Y. L.; Akopyan, M. E.; Vilesov, F. I.; Chizhov, Y. V. Photoionization processes in gaseous cyclohexane, and chloro-and bromocyclohexane. *High Energy Chem.* **1973**, *7*, 340.
(24) Petrone, D. A.; Ye, J.; Lautens, M. Modern transition-metal-catalyzed carbon-halogen bond formation. *Chem. Rev.* **2016**, *116*, 8003−8104.
(25) Cavallo, G.; Metrangolo, P.; Milani, R.; Pilati, T.; Priimagi, A.; Resnati, G.; Terraneo, G. The halogen bond. *Chem. Rev.* **2016**, *116*, 2478−2601.
(26) Paunović, V.; Zichittella, G.; Moser, M.; Amrute, A. P.; Pérez-Ramírez, J. Catalyst design for natural-gas upgrading through oxybromination chemistry. *Nat. Chem.* **2016**, *8*, 803−809.
(27) Paunović, V.; Hemberger, P.; Bodi, A.; López, N.; Pérez-Ramírez, J. Evidence of radical chemistry in catalytic methane oxybromination. *Nat. Catal.* **2018**, *1*, 363−370.
(28) Ruscic, B.; Bross, D. H. Active Thermochemical Tables (ATcT) Values based on ver. 1.122p of the Thermochemical Network. 2020. Available at ATcT.anl.gov, (accessed October 1, 2020).
(29) Johnson, M.; Bodi, A.; Schulz, L.; Gerber, T. Vacuum ultraviolet beamline at the swiss light source for chemical dynamics studies. *Nucl. Instrum. Methods Phys. Res., Sect. A* **2009**, *610*, 597−603.
(30) Sztáray, B.; Voronova, K.; Torma, K. G.; Covert, K. J.; Bodi, A.; Hemberger, P.; Gerber, T.; Osborn, D. L. CRF-PEPICO: Double velocity map imaging photoelectron photoion coincidence spectroscopy for reaction kinetics studies. *J. Chem. Phys.* **2017**, *147*, 013944.
(31) Sztáray, B.; Baer, T. Suppression of hot electrons in threshold photoelectron photoion coincidence spectroscopy using velocity focusing optics. *Rev. Sci. Instrum.* **2003**, *74*, 3763−3768.
(32) Bodi, A.; Sztáray, B.; Baer, T.; Johnson, M.; Gerber, T. Data acquisition schemes for continuous two-particle time-of-flight coincidence experiments. *Rev. Sci. Instrum.* **2007**, *78*, 084102.
(33) Bodi, A.; Baer, T.; Wells, N. K.; Fakhoury, D.; Klecyngier, D.; Kercher, J. P. Controlling tunnelling in methane loss from acetone ions by deuteration. *Phys. Chem. Chem. Phys.* **2015**, *17*, 28505−28509.
(34) Rice, O. K.; Ramsperger, H. C. Theories of unimolecular gas reactions at low pressures. *J. Am. Chem. Soc.* **1927**, *49*, 1617−1629.
(35) Rice, O. K.; Ramsperger, H. C. Theories of unimolecular gas reactions at low pressures. Ii. *J. Am. Chem. Soc.* **1928**, *50*, 617−620.
(36) Marcus, R. A.; Rice, O. K. The kinetics of the recombination of methyl radicals and iodine atoms. *J. Phys. Chem.* **1951**, *55*, 894−908.
(37) Curtiss, L. A.; Redfern, P. C.; Raghavachari, K. Gaussian-4 theory. *J. Chem. Phys.* **2007**, *126*, 084108.
(38) Tech, J. L. Analysis of the spectrum of neutral atomic bromine (Br I). *J. Res. Natl. Bur. Stand., Sect. A* **1963**, *67A*, 505−554.
(39) Frisch, M. J.; Trucks, G. W.; Schlegel, H. B.; Scuseria, G. E.; Robb, M. A.; Cheeseman, J. R.; Scalmani, G.; Barone, V.; Mennucci, B.; Petersson, G. A.; et al. *Gaussian 16* Revision A.03; Gaussian, Inc.: Wallingford CT, 2016.
(40) Martin, J. M. L.; de Oliveira, G. Towards standard methods for benchmark quality ab initio thermochemistry-W1 and W2 theory. *J. Chem. Phys.* **1999**, *111*, 1843−1856.
(41) Montgomery, J. A.; Frisch, M. J.; Ochterski, J. W.; Petersson, G. A. A complete basis set model chemistry. VII. Use of the minimum population localization method. *J. Chem. Phys.* **2000**, *112*, 6532−6542.
(42) Pritchard, B. P.; Altarawy, D.; Didier, B.; Gibson, T. D.; Windus, T. L. New basis set exchange: An open, up-to-date resource for the molecular sciences community. *J. Chem. Inf. Model.* **2019**, *59*, 4814−4820.
(43) Wu, X.; Tang, G.; Zhang, H.; Zhou, X.; Liu, S.; Liu, F.; Sheng, L.; Yan, B. Cl-Loss dynamics in the dissociative photoionization of CF3Cl with threshold photoelectron-photoion coincidence imaging. *Phys. Chem. Chem. Phys.* **2018**, *20*, 4917−4925.
(44) Wu, X.; Yu, T.; Chen, Y.; Zhou, X.; Liu, S.; Dai, X.; Liu, F.; Sheng, L. Dissociative photoionization of CF3Cl via the C2E and D2E states: competition of the C-F and C-Cl bond cleavages. *Phys. Chem. Chem. Phys.* **2019**, *21*, 4998−5005.
(45) Harvey, J.; Bodi, A.; Tuckett, R. P.; Sztáray, B. Dissociation dynamics of fluorinated ethene cations: From time bombs on a molecular level to double-regime dissociators. *Phys. Chem. Chem. Phys.* **2012**, *14*, 3935−3948.
(46) Voronova, K.; Torma, K. G.; Kercher, J. P.; Bodi, A.; Sztáray, B. Dissociative photoionization of chromium hexacarbonyl: A round-trip ticket to non-statisticality and a detective story in thermochemistry. *Int. J. Mass spectrom.* **2019**, *438*, 63−71.
(47) Bodi, A.; Kvaran, Á.; Sztáray, B. Thermochemistry of Halomethanes CFnBr4-n(n= 0-3) Based on iPEPICO Experiments and Quantum Chemical Computations. *J. Phys. Chem. A* **2011**, *115*, 13443−13451.
(48) West, B.; Joblin, C.; Blanchet, V.; Bodi, A.; Sztáray, B.; Mayer, P. M. On the dissociation of the naphthalene radical cation: New ipepico and tandem mass spectrometry results. *J. Phys. Chem. A* **2012**, *116*, 10999−11007.
(49) Heringa, M. F.; Slowik, J. G.; Prévôt, A. S. H.; Baltensperger, U.; Hemberger, P.; Bodi, A. Dissociative ionization mechanism and appearance energies in adipic acid revealed by imaging photoelectron photoion coincidence, selective deuteration, and calculations. *J. Phys. Chem. A* **2016**, *120*, 3397−3405.
(50) Majer, K.; Signorell, R.; Heringa, M. F.; Goldmann, M.; Hemberger, P.; Bodi, A. Valence photoionization of thymine: Ionization energies, vibrational structure, and fragmentation pathways from the slow to the ultrafast. *Chem.—Eur. J.* **2019**, *25*, 14192−14204.
(51) Weidner, P.; Voronova, K.; Bodi, A.; Sztáray, B. Dissociative photoionization of 1,3-dioxolane: We need six channels to fit the elephant. *J. Mass Spectrom.* **2020**, *55*, No. e4522.
(52) Bouwman, J.; Sztáray, B.; Oomens, J.; Hemberger, P.; Bodi, A. Dissociative photoionization of quinoline and isoquinoline. *J. Phys. Chem. A* **2015**, *119*, 1127−1136.
(53) Lang, M.; Holzmeier, F.; Hemberger, P.; Fischer, I. Threshold Photoelectron Spectra of Combustion Relevant C4H5 and C4H7 Isomers. *J. Phys. Chem. A* **2015**, *119*, 3995−4000.
(54) Olah, G. A.; Bollinger, J. M.; Cupas, C. A.; Lukas, J. Stable carbonium ions. XXXIV. 1-Methylcyclopentyl cation. *J. Am. Chem. Soc.* **1967**, *89*, 2692.
(55) Lias, S. G.; Shold, D. M.; Ausloos, P. Proton-transfer reactions involving alkyl ions and alkenes. Rate constants, isomerization processes, and the derivation of thermochemical data. *J. Am. Chem. Soc.* **1980**, *102*, 2540−2548.
(56) Radziemski, L. J.; Kaufman, V. Wavelengths, Energy Levels, and Analysis of Neutral Atomic Chlorine (Cl i). *J. Opt. Soc. Am.* **1969**, *59*, 424−443.
(57) Luc-Koenig, E.; Morillon, C.; Vergès, J. Etude Expérimentale et Théorique de l'Iode Atomique.Observation du Spectre d'Arc Infrarouge, Classification et Structure Hyperfine. *Phys. Scr.* **1975**, *12*, 199−219.
(58) Hunter, E. P. L.; Lias, S. G. Evaluated gas phase basicities and proton affinities of molecules: An update. *J. Phys. Chem. Ref. Data* **1998**, *27*, 413−656.

https://dx.doi.org/10.1021/acs.jpca.0c10386
J. Phys. Chem. A 2021, 125, 646−656

(59) Steele, W. V.; Chirico, R. D.; Knipmeyer, S. E.; Nguyen, A.; Smith, N. K.; Tasker, I. R. Thermodynamic properties and ideal-gas enthalpies of formation for cyclohexene, phthalan (2,5-dihydrobenzo-3,4-furan), isoxazole, octylamine, dioctylamine, trioctylamine, phenyl isocyanate, and 1,4,5,6-tetrahydropyrimidine. *J. Chem. Eng. Data* **1996**, *41*, 1269−1284.
(60) Chase, M. *NIST—JANAF Thermochemical Tables (Journal of Physical and Chemical Reference Data Monograph no. 9)*, 4th ed.; American Institute of Physics: Washington DC 1998.
(61) An, X.-W.; Guo, D.-J. Formation enthalpies and non-bonding interactions of hexachlorocyclohexanes. *Thermochim. Acta* **1995**, *253*, 235−242.
(62) Good, W. D.; Smith, N. K. Enthalpies of combustion of toluene, benzene, cyclohexane, cyclohexene, methylcyclopentane, 1-methylcyclopentene, and n-hexane. *J. Chem. Eng. Data* **1969**, *14*, 102−106.
(63) Majer, V.; Svoboda, V.; Kehiaian, H. V. *Enthalpies of Vaporization of Organic Compounds: A Critical Review and Data Compilation*; Blackwell Scientific Oxford: 1985; Vol. *32*.
(64) Chai, J.-D.; Head-Gordon, M. Long-range corrected hybrid density functionals with damped atom-atom dispersion corrections. *Phys. Chem. Chem. Phys.* **2008**, *10*, 6615−6620.
(65) Bergner, A.; Dolg, M.; Küchle, W.; Stoll, H.; Preuss, H. Ab initio energy-adjusted pseudopotentials for elements of groups 13-17. *Mol. Phys.* **1993**, *80*, 1431−1441.
(66) Martin, J. M. L.; Sundermann, A. Correlation consistent valence basis sets for use with the stuttgart-dresden-bonn relativistic effective core potentials: The atoms Ga-Kr and In-Xe. *J. Chem. Phys.* **2001**, *114*, 3408−3420.
(67) Zhao, Y.; Truhlar, D. G. The M06 suite of density functionals for main group thermochemistry, thermochemical kinetics, noncovalent interactions, excited states, and transition elements: Two new functionals and systematic testing of four M06-class functionals and 12 other functionals. *Theor. Chem. Acc.* **2008**, *120*, 215−241.
(68) Grimme, S.; Antony, J.; Ehrlich, S.; Krieg, H. A consistent and accurate ab initio parametrization of density functional dispersion correction (DFT-D) for the 94 elements H-Pu. *J. Chem. Phys.* **2010**, *132*, 154104.
(69) Peterson, K. A.; Figgen, D.; Goll, E.; Stoll, H.; Dolg, M. Systematically convergent basis sets with relativistic pseudopotentials. II. Small-core pseudopotentials and correlation consistent basis sets for the post-d group 16-18 elements. *J. Chem. Phys.* **2003**, *119*, 11113.
(70) Breugst, M.; Detmar, E.; von der Heiden, D. Origin of the catalytic effects of molecular iodine: A computational analysis. *ACS Catal.* **2016**, *6*, 3203−3212.
(71) Perdew, J. P.; Burke, K.; Ernzerhof, M. Generalized gradient approximation made simple. *Phys. Rev. Lett.* **1996**, *77*, 3865−3868.
(72) Perdew, J. P.; Burke, K.; Ernzerhof, M. Generalized Gradient Approximation Made Simple [Phys. Rev. Lett. 77, 3865 (1996)]. *Phys. Rev. Lett.* **1997**, *78*, 1396.
(73) Weigend, F.; Ahlrichs, R. Balanced basis sets of split valence, triple zeta valence and quadruple zeta valence quality for H to Rn: Design and assessment of accuracy. *Phys. Chem. Chem. Phys.* **2005**, *7*, 3297−3305.
(74) Becker, P.; Duhamel, T.; Stein, C. J.; Reiher, M.; Muñiz, K. Cooperative Light-Activated Iodine and Photoredox Catalysis for the Amination of Csp3 −H Bonds. *Angew. Chem., Int. Ed.* **2017**, *56*, 8004−8008.
(75) Karton, A.; Tarnopolsky, A.; Lamère, J.-F.; Schatz, G. C.; Martin, J. M. L. Highly Accurate First-Principles Benchmark Data Sets for the Parametrization and Validation of Density Functional and Other Approximate Methods. Derivation of a Robust, Generally Applicable, Double-Hybrid Functional for Thermochemistry and Thermochemical Kinetics†. *J. Phys. Chem. A* **2008**, *112*, 12868−12886.
(76) Han, S.; Yoo, H. S.; Kim, S. K. Conformer-specific ionization spectroscopy of bromocyclohexane: Equatorial versus axial conformers. *J. Phys. Chem. A* **2010**, *114*, 10005−10010.
(77) Cioslowski, J. A new population analysis based on atomic polar tensors. *J. Am. Chem. Soc.* **1989**, *111*, 8333−8336.

https://dx.doi.org/10.1021/acs.jpca.0c10386
J. Phys. Chem. A 2021, 125, 646−656